

Manipulation of ultracold atoms in dressed adiabatic radio frequency potentials

I. Lesanovsky,^{1,2,*} S. Hofferberth,¹ J. Schmiedmayer,^{1,3} and Peter Schmelcher^{4,5,†}

¹*Physikalisches Institut, Universität Heidelberg, D-69120 Heidelberg, Germany*

²*Institute of Electronic Structure and Laser, Foundation for Research and Technology - Hellas, P.O. Box 1527, GR-711 10 Heraklion, Greece*

³*Atominstitut Österreichischer Universitäten, TU-Wien, Vienna, Austria*

⁴*Physikalisches Institut, Universität Heidelberg, Philosophenweg 12, 69120 Heidelberg, Germany*

⁵*Theoretische Chemie, Institut für Physikalische Chemie,*

Universität Heidelberg, INF 229, 69120 Heidelberg, Germany

(Dated: July 7, 2018)

We explore properties of atoms whose magnetic hyperfine sub-levels are coupled by an external magnetic radio frequency (rf) field. We perform a thorough theoretical analysis of this driven system and present a number of systematic approximations which eventually give rise to dressed adiabatic radio frequency potentials. The predictions of this analytical investigation are compared to numerically exact results obtained by a wave packet propagation. We outline the versatility and flexibility of this new class of potentials and demonstrate their potential use to build atom optical elements such as double-wells, interferometers and ringtraps. Moreover, we perform simulations of interference experiments carried out in rf induced double-well potentials. We discuss how the nature of the atom-field coupling mechanism gives rise to a decrease of the interference contrast.

PACS numbers: 03.75.Be, 32.80.Pj, 42.50.Vk

I. INTRODUCTION

Using static magnetic fields in order to gain control over the motion of neutral ground state atoms is a well-established and frequently used experimental technique [1, 2, 3, 4, 5]. In particular for the manipulation of gases of atoms in the thermal and the quantum degenerate regime magnetic fields have been successfully employed [6]. In the adiabatic approximation the atoms are subjected to a potential which is proportional to the modulus of the magnetic field [4, 7]. Hence, since the field generating structures can be almost designed at will there seems in principle to exist a total freedom in designing potential 'landscapes' [4, 8]. This virtual flexibility has resulted in numerous proposals about how to design atom-optical elements such as traps, guides and also interferometers [5, 9, 10, 11, 12, 13]. However, Maxwell's equations prevent magnetic traps from being designed entirely arbitrarily. Earnshaw's theorem for instance states that there are no local magnetic field maxima allowed to occur inside a source-free region of space. This puts significant constraints onto the magnetic field shapes and thus on the trapping potentials. These restrictions can be circumvented by superimposing time-dependent magnetic field components on the static fields. This give rise to adiabatic potentials which show an enormous flexibility and versatility [14, 15, 16, 17, 18, 19, 20]. With the support of such time-dependent fields one can create even complicated geometries such as rings and interferometers with comparatively little effort. Such atom optical elements are ideal tools to study interference [16, 21] and tunneling [22] of Bose-Einstein Condensates.

In this paper we discuss in detail the theoretical foundations of the adiabatic potentials that emerge if the magnetic hyperfine states of an alkali atom are being coupled by an external radio frequency (rf) field. In Sec. II we present the underlying Hamiltonian as well as a number of transformations and approximations which eventually give rise to the adiabatic potentials which we present in Sec. III. These general considerations are followed by the discussion of a specific field configuration in Sec. IV. We demonstrate how a very simple setup consisting of a Ioffe-Pritchard trap [23] and two linearly polarized rf fields allow one to create a number of atom optical elements. In particular we outline the realization of a tunable double well as well as a ring trap. These analytical results are confirmed by a numerical wave packet propagation which utilizes the exact spinor Hamiltonian. In Sec. V we discuss interference experiments which are carried out by using an rf induced double-well. We outline how the atom-field coupling which essentially forms the rf potentials influences the outcome of interference experiments. In particular we find an oscillation of the interference phase and a reduction of contrast. We conclude and summarize our findings in Sec. VI.

*Electronic address: lesanovsky@atomchip.org

†Electronic address: Peter.Schmelcher@pci.uni-heidelberg.de

II. GENERAL HAMILTONIAN OF RADIO FREQUENCY COUPLED HYPERFINE SUB-STATES

The ground state and the first few excited states of an alkali atom are substantially split into several hyperfine-manifolds being usually labeled by the quantum number F . In the presence of a magnetic field $\mathbf{B}(\mathbf{r}, t)$ each of these manifolds again splits into $2F + 1$ branches. Let us assume the field to be of moderate strength, i.e. not to couple adjacent hyperfine-manifolds. In this case the dynamics of an atom within a single manifold is governed by the Hamiltonian

$$H = \frac{\mathbf{p}^2}{2M} + g_F \mu_B \mathbf{F} \cdot \mathbf{B}(\mathbf{r}, t). \quad (1)$$

Here M is the atomic mass, \mathbf{F} the $2F + 1$ -dimensional representation of the angular momentum operator and g_F the corresponding g -factor. We assume the magnetic field to decompose according to

$$\mathbf{B}(\mathbf{r}, t) = \mathbf{B}_S(\mathbf{r}) + \mathbf{B}_{\text{RF}}(\mathbf{r}, t) = \mathbf{B}_S(\mathbf{r}) + \sum_n \mathbf{B}_n(\mathbf{r}) \cos(\omega t - \delta_n). \quad (2)$$

The static field $\mathbf{B}_S(\mathbf{r})$ serves for the purpose of trapping, i.e. there are trapped states even in the absence of the field $\mathbf{B}_{\text{RF}}(\mathbf{r}, t)$ being a monochromatic radio frequency (rf) field which is used to couple the different magnetic hyperfine sub-states.

The static magnetic field vector $\mathbf{B}_S(\mathbf{r})$ defines a natural quantization axis which we refer to as the z -axis. To manifest this in the following we construct a unitary transformation that rotates the angular momentum vector \mathbf{F} such that it is aligned with the local magnetic field vector. Such a transformation which in general depends on the position \mathbf{r} of the atom is given by

$$U_S(\mathbf{r}) = \exp[-iF_z \alpha(\mathbf{r})] \exp[-iF_y \beta(\mathbf{r})] \quad (3)$$

with the angles

$$\alpha(\mathbf{r}) = \arctan \left[\frac{B_{S_y}(\mathbf{r})}{B_{S_x}(\mathbf{r})} \right] \quad \text{and} \quad \beta(\mathbf{r}) = \arctan \left[\frac{\sqrt{B_{S_x}^2(\mathbf{r}) + B_{S_y}^2(\mathbf{r})}}{B_{S_z}(\mathbf{r})} \right]. \quad (4)$$

Applying $U_S(\mathbf{r})$ to the static atom-field coupling term of the Hamiltonian (1) yields

$$\begin{aligned} U_S^\dagger(\mathbf{r}) \mathbf{F} U_S(\mathbf{r}) \cdot \mathbf{B}_S(\mathbf{r}) &= \{\mathfrak{R}_y[-\beta(\mathbf{r})] \mathfrak{R}_z[-\alpha(\mathbf{r})] \mathbf{F}\} \cdot \mathbf{B}_S(\mathbf{r}) \\ &= \mathbf{F} \cdot \{\mathfrak{R}_y[\beta(\mathbf{r})] \mathfrak{R}_z[\alpha(\mathbf{r})] \mathbf{B}_S(\mathbf{r})\} = F_z |\mathbf{B}_S(\mathbf{r})|. \end{aligned} \quad (5)$$

As is seen here $U_S(\mathbf{r})$ indeed performs the requested operation since the coupling to the static field has become proportional to F_z . The rotation induced by $U_S(\mathbf{r})$ can be equivalently expressed in terms of the rotation matrices $\mathfrak{R}_i[\phi]$ acting on the vector \mathbf{F} . Here ϕ is the rotation angle and the index i denotes the axis around which the vector is being rotated. However, instead of rotating \mathbf{F} one can equally rotate the magnetic field vector which leads to the same result. This is exploited in the second last equality in the series of equations (5). Consequently, applying $U_S(\mathbf{r})$ to the Hamiltonian (1) yields

$$U_S^\dagger(\mathbf{r}) H U_S(\mathbf{r}) = U_S^\dagger(\mathbf{r}) \frac{\mathbf{p}^2}{2M} U_S(\mathbf{r}) + g_F \mu_B F_z |\mathbf{B}_S(\mathbf{r})| + g_F \mu_B \sum_n \bar{\mathbf{B}}_n(\mathbf{r}) \cdot \mathbf{F} \cos(\omega t - \delta_n) \quad (6)$$

with $\bar{\mathbf{B}}_n(\mathbf{r}) = \mathfrak{R}_y[\beta(\mathbf{r})] \mathfrak{R}_z[\alpha(\mathbf{r})] \mathbf{B}_n(\mathbf{r})$. Here the $\bar{\mathbf{B}}_n(\mathbf{r})$ are the amplitude vectors of the rf fields now seen from a coordinate system in which the static field $\mathbf{B}_S(\mathbf{r})$ defines the z -axis.

We now apply a second unitary transformation

$$U_R = \exp \left[-i \frac{g_F}{|g_F|} F_z \omega t \right] \quad (7)$$

which transfers us into a frame that rotates around the z -axis (local quantization axis) with the angular velocity ω . Transforming the time derivative of the Schrödinger equation according to

$$U_R^\dagger \partial_t U_R = \partial_t + U_R^\dagger (\partial_t U_R) \quad (8)$$

one finds the effective Hamiltonian

$$\begin{aligned}
H_{\text{eff}} &= U_R^\dagger U_S^\dagger(\mathbf{r}) \frac{\mathbf{p}^2}{2M} U_S(\mathbf{r}) U_R + g_F \mu_B \left[|\mathbf{B}_S(\mathbf{r})| - \frac{g_F}{|g_F|} \frac{\hbar\omega}{g_F \mu_B} \right] F_z \\
&\quad + \frac{g_F \mu_B}{2} \sum_n \left[\left\{ \left[\mathfrak{R}_z[-\zeta_n] + \mathfrak{R}_z \left[\zeta_n - 2 \frac{g_F}{|g_F|} \omega t \right] \right] \bar{\mathbf{B}}_n(\mathbf{r}) \right\} \cdot \mathbf{F} - \bar{B}_{nz}(\mathbf{r}) F_z \right] \\
&\quad + g_F \mu_B \sum_n \bar{B}_{nz}(\mathbf{r}) \cos(\omega t - \delta_n) F_z.
\end{aligned} \tag{9}$$

with the phase-angle $\zeta_n = \frac{g_F}{|g_F|} \delta_n$.

In the next step we remove the last term in the Hamiltonian, which oscillates at the frequency ω . This can be done by applying the series of unitary transformations

$$\begin{aligned}
U_T(\mathbf{r}, t) &= \exp \left[-i \frac{g_F \mu_B}{\hbar\omega} \sum_n \bar{B}_{nz}(\mathbf{r}) \sin(\omega t - \delta_n) F_z \right] \\
&= \prod_n \exp \left[-i \frac{g_F \mu_B}{\hbar\omega} \bar{B}_{nz}(\mathbf{r}) \sin(\omega t - \delta_n) F_z \right] = \prod_n U_{Tn}(\mathbf{r}, t)
\end{aligned} \tag{10}$$

to the time-dependent Schrödinger equation. They have to be carried out in accordance with equation (8). Since $U_T(\mathbf{r}, t)$ depends on F_z it does not only remove the unwanted last term of H_{eff} but also introduces additional ones arising from the transformation of F_x and F_y . To see this we apply $U_{Tn}(\mathbf{r}, t)$ to the operator \mathbf{F} which results in

$$\begin{aligned}
U_{Tn}^\dagger(\mathbf{r}, t) \mathbf{F} U_{Tn}(\mathbf{r}, t) &= \mathfrak{R}_z \left[-\frac{g_F \mu_B}{\hbar\omega} \bar{B}_{zn}(\mathbf{r}) \sin(\omega t - \delta_n) \right] \mathbf{F} \\
&= \mathfrak{R}_z [-\gamma_n(\mathbf{r}) \sin(\omega t - \delta_n)] \mathbf{F} \\
&= J_0[\gamma_n(\mathbf{r})] \mathbf{F} + 2 \sum_{m=1}^{\infty} J_{2m}[\gamma_n(\mathbf{r})] \cos(2m[\omega t - \delta_n]) \mathbf{F} \\
&\quad + 2 \mathfrak{R}_z \left[-\frac{\pi}{2} \right] \sum_{m=0}^{\infty} J_{2m+1}[\gamma_n(\mathbf{r})] \sin([2m+1][\omega t - \delta_n]) \mathbf{F}
\end{aligned} \tag{11}$$

with $J_m[x]$ being the Bessel functions of the first kind and $\gamma_n(\mathbf{r}) = \frac{g_F \mu_B}{\hbar\omega} \bar{B}_{zn}(\mathbf{r})$. Since $U_T(\mathbf{r}, t)$ in general depends on the spatial coordinate the Hamiltonian which emerges by transforming H_{eff} reads

$$\begin{aligned}
H_{\text{RF}} &= \frac{1}{2M} [\mathbf{p} + \mathbf{A}(\mathbf{r}, t)]^2 + g_F \mu_B \left[|\mathbf{B}_S(\mathbf{r})| - \frac{g_F}{|g_F|} \frac{\hbar\omega}{g_F \mu_B} \right] F_z \\
&\quad + \frac{g_F \mu_B}{2} \sum_n \left[\left\{ \left[\mathfrak{R}_z[-\zeta_n] + \mathfrak{R}_z \left[\zeta_n - 2 \frac{g_F}{|g_F|} \omega t \right] \right] \bar{\mathbf{B}}_n(\mathbf{r}) \right\} \cdot U_T^\dagger(\mathbf{r}, t) \mathbf{F} U_T(\mathbf{r}, t) - \bar{B}_{nz}(\mathbf{r}) F_z \right].
\end{aligned} \tag{12}$$

with the gauge potential

$$\mathbf{A}(\mathbf{r}, t) = U^\dagger(\mathbf{r}, t) (\mathbf{p} U(\mathbf{r}, t)) \tag{13}$$

and the abbreviation $U(\mathbf{r}, t) = U_S(\mathbf{r}) U_T(\mathbf{r}, t)$ for the combined static and time-dependent transformation.

III. DRESSED ADIABATIC RADIO FREQUENCY INDUCED POTENTIALS

Since we have performed only unitary transformations the two Hamiltonians (12) and (1) are equivalent. At first glance it is not obvious that much has been gained since the Hamiltonian (12) appears to be extremely unhandy. However, we will show that equation (12) serves as an excellent basis for performing a number of approximation. Finally it will allow us to derive a time-independent expression for the dressed adiabatic potentials.

For the first approximation we assume

$$\gamma_n(\mathbf{r}) = \left| \frac{g_F \mu_B}{\hbar\omega} \bar{B}_{zn}(\mathbf{r}) \right| \ll 1, \tag{14}$$

i.e. the Larmor frequency $\omega_{L\parallel} = |g_F\mu_B\bar{B}_{nz}(\mathbf{r})|$ associated with the z -component of the n -th rf field (in the frame aligned with the vector $\mathbf{B}_S(\mathbf{r})$) is small compared to the rf frequency. In this case we can approximate

$$J_i[\gamma_n(\mathbf{r})] \approx \begin{cases} 1 & \text{if } i = 0 \\ 0 & \text{if } i \neq 0 \end{cases}. \quad (15)$$

This allows us to replace $U_T^\dagger(\mathbf{r}, t)\mathbf{F}U_T(\mathbf{r}, t)$ in equation (12) by \mathbf{F} itself, yielding a major simplification. As long as $\omega \gg \omega_{L\parallel}$ the oscillating motion of the field amplitude will dominate the Larmor precession around the magnetic field vector. Later on we will see that even if $\omega \gg \omega_{L\parallel}$ is not strictly satisfied, i.e. both frequencies differ only by one order of magnitude, the above approximation works surprisingly well.

In the next step we utilize the so-called rotating-wave-approximation which essentially consists of the negligence of all terms that oscillate rapidly with a frequency 2ω . Accounting for equation (15) this give rise to the Hamiltonian

$$\begin{aligned} H_{\text{RF}} &= \frac{1}{2M} [\mathbf{p} + \mathbf{A}(\mathbf{r}, t)]^2 + g_F\mu_B \left[|\mathbf{B}_S(\mathbf{r})| - \frac{g_F}{|g_F|} \frac{\hbar\omega}{g_F\mu_B} \right] F_z \\ &\quad + \frac{g_F\mu_B}{2} \sum_n \left[\{\mathfrak{R}_z[-\zeta_n] \bar{\mathbf{B}}_n(\mathbf{r})\} \cdot \mathbf{F} - \bar{B}_{nz}(\mathbf{r}) F_z \right] \\ &= \frac{1}{2M} [\mathbf{p} + \mathbf{A}(\mathbf{r}, t)]^2 + g_F\mu_B \mathbf{B}_{\text{eff}}(\mathbf{r}) \cdot \mathbf{F} \end{aligned} \quad (16)$$

The dynamics of the spin particle is thus effectively determined by a Hamiltonian which consists of two gauge potentials $\mathbf{A}(\mathbf{r}, t)$ and $\Phi(\mathbf{r}, t)$ and a coupling to an effective magnetic field whose components read

$$B_{\text{eff}x}(\mathbf{r}) = \frac{1}{2} \sum_n \{\mathfrak{R}_z[-\zeta_n] \bar{\mathbf{B}}_n(\mathbf{r})\}_x \quad (17)$$

$$B_{\text{eff}y}(\mathbf{r}) = \frac{1}{2} \sum_n \{\mathfrak{R}_z[-\zeta_n] \bar{\mathbf{B}}_n(\mathbf{r})\}_y \quad (18)$$

$$B_{\text{eff}z}(\mathbf{r}) = |\mathbf{B}_S(\mathbf{r})| - \frac{\hbar\omega}{|g_F|\mu_B}. \quad (19)$$

Apart from the gauge potentials the new time-independent Hamiltonian has acquired the same form as our initial Hamiltonian (1) but with a static effective magnetic field. The main advantage is now that \mathbf{B}_{eff} is not to satisfy Maxwell's equations since it is no true magnetic field. *This is exactly the reason why combined static and rf fields permit the design of a much larger variety of traps than it is possible by solely using static fields.* Moreover, the dependence of the ζ_n on the sign of the atomic g -factor enables one to realize state-dependent potentials as outlined in Ref. [17].

To obtain the adiabatic rf potentials we diagonalize the last term of the Hamiltonian (16) by applying the transformation

$$U_F(\mathbf{r}) = \exp[-iF_z\tilde{\alpha}(\mathbf{r})] \exp[-iF_y\tilde{\beta}(\mathbf{r})]. \quad (20)$$

This transformation is similar to the one given by equation (3) but with the rotation angles $\tilde{\alpha}(\mathbf{r})$ and $\tilde{\beta}(\mathbf{r})$ now being defined as

$$\tilde{\alpha}(\mathbf{r}) = \arctan \left[\frac{B_{\text{eff}y}(\mathbf{r})}{B_{\text{eff}x}(\mathbf{r})} \right] \quad \text{and} \quad \tilde{\beta}(\mathbf{r}) = \arctan \left[\frac{\sqrt{B_{\text{eff}x}^2(\mathbf{r}) + B_{\text{eff}y}^2(\mathbf{r})}}{B_{\text{eff}z}(\mathbf{r})} \right]. \quad (21)$$

Essentially this leads to the Hamiltonian

$$H_{\text{final}} = \frac{1}{2M} [\mathbf{p} + \mathbf{A}'(\mathbf{r}, t)]^2 + g_F\mu_B |\mathbf{B}_{\text{eff}}(\mathbf{r})| F_z \quad (22)$$

with the new gauge field $\mathbf{A}'(\mathbf{r}, t)$ being defined according to equation (13) but with the transformation $U(\mathbf{r}, t)$ being replaced by $U'(\mathbf{r}, t) = U_S(\mathbf{r})U_T(\mathbf{r}, t)U_F(\mathbf{r})$.

Finally we perform the adiabatic approximation which, just like for static magnetic traps [4, 24], essentially consists of neglecting the gauge potential $\mathbf{A}'(\mathbf{r}, t)$. This yields the adiabatic Hamiltonian

$$H_{\text{ad}} = \frac{\mathbf{p}^2}{2M} + g_F\mu_B |\mathbf{B}_{\text{eff}}(\mathbf{r})| F_z = \frac{\mathbf{p}^2}{2M} + V_{\text{ad}}(\mathbf{r}) \quad (23)$$

with dressed adiabatic radio frequency induced potentials

$$V_{\text{ad}}(\mathbf{r}) = m_F g_F \mu_B \left[\left(|\mathbf{B}_S(\mathbf{r})| - \frac{\hbar\omega}{|g_F \mu_B|} \right)^2 + B_{\text{eff}_x}^2(\mathbf{r}) + B_{\text{eff}_y}^2(\mathbf{r}) \right]^{\frac{1}{2}}. \quad (24)$$

These potentials are time-independent and turn out to be extremely versatile in terms of their applicability. Of course the validity of the approximation utilized in this section has to be ensured. However, it is hard to discuss this in general and has therefore to be checked for the individual field setup. In the next section we will restrict our considerations to a specific case.

IV. TWO-DIMENSIONAL RF POTENTIALS

Let us now demonstrate how a very simple and easy to build experimental setup can give rise to extremely versatile dressed adiabatic potentials that can be used for building atom optical elements such as beam-splitters and interferometers.

To this end we consider two-dimensional potentials which are generated from a static Ioffe trap whose field is given by

$$\mathbf{B}_S(\mathbf{r}) = Gx\mathbf{e}_x - Gy\mathbf{e}_y + B_I\mathbf{e}_z. \quad (25)$$

This two-dimensional trapping field shall be superimposed by two homogeneous and mutually orthogonal radio-frequency fields

$$\mathbf{B}_1(\mathbf{r}) = \frac{B_{\text{RF}}}{\sqrt{2}}\mathbf{e}_x \quad \text{and} \quad \mathbf{B}_2(\mathbf{r}) = \frac{B_{\text{RF}}}{\sqrt{2}}\mathbf{e}_y. \quad (26)$$

We choose the corresponding phase angles to be $\delta_1 = 0$ and $\delta_2 = \delta$. After inserting this fields the Hamiltonian (1) becomes

$$H_{2\text{RF}}(t) = \frac{\mathbf{p}^2}{2M} + g_F \mu_B \left[\left[Gx + \frac{B_{\text{RF}}}{\sqrt{2}} \cos \omega t \right] F_x - \left[Gy - \frac{B_{\text{RF}}}{\sqrt{2}} \cos(\omega t - \delta) \right] F_y + B_I F_z \right]. \quad (27)$$

The goal of the following discussion is two-fold: Firstly we will calculate the dressed adiabatic potentials arising from the spin-field coupling term of the Hamiltonian (27). We will point out the flexibility of this rather simple field configuration which enables one to create a number of atom optical elements. Secondly we want to compare our results to a numerically exact wave packet propagation that is governed by the Schrödinger equation

$$i\hbar\partial_t |\Psi(t)\rangle = H_{2\text{RF}}(t) |\Psi(t)\rangle. \quad (28)$$

A. Adiabatic potentials

In order to calculate the dressed adiabatic potentials we need to construct and apply the unitary transformation (3) to the Hamiltonian (1). With the rf fields (27) the corresponding angles read

$$\alpha(\mathbf{r}) = \arctan \left[-\frac{y}{x} \right] \quad \text{and} \quad \beta(\mathbf{r}) = \arctan \left[\frac{G}{B_I} \sqrt{x^2 + y^2} \right]. \quad (29)$$

Employing cylindrical coordinates the rotation matrices given by equation (5) read

$$\mathfrak{R}_y[\beta(\mathbf{r})] \mathfrak{R}_z[\alpha(\mathbf{r})] = \begin{pmatrix} \frac{B_I}{\sqrt{B_I^2 + G^2 \rho^2}} & 0 & -\frac{G\rho}{\sqrt{B_I^2 + G^2 \rho^2}} \\ 0 & 1 & 0 \\ \frac{G\rho}{\sqrt{B_I^2 + G^2 \rho^2}} & 0 & \frac{B_I}{\sqrt{B_I^2 + G^2 \rho^2}} \end{pmatrix} \begin{pmatrix} \cos \phi & -\sin \phi & 0 \\ \sin \phi & \cos \phi & 0 \\ 0 & 0 & 1 \end{pmatrix} \quad (30)$$

with the polar angle ϕ and the radius ρ . According to equation (24) we then find the following dressed adiabatic potential:

$$\frac{V_{\text{ad}}(\mathbf{r})}{m_F g_F \mu_B} = \left[\left(|\mathbf{B}_S(\mathbf{r})| - \frac{\hbar\omega}{|g_F \mu_B|} \right)^2 + \frac{B_{\text{RF}}^2}{4} \left(1 + \frac{B_I \sin \delta}{|\mathbf{B}_S(\mathbf{r})|} + \frac{G^2 \rho^2}{2|\mathbf{B}_S(\mathbf{r})|^2} (\cos \delta \sin(2\phi) - 1) \right) \right]^{\frac{1}{2}}. \quad (31)$$

For $\cos \delta > 0$ we find the minima and maxima of the potential at $\phi_{\min} = \frac{3}{4}\pi, \frac{7}{4}\pi$ and $\phi_{\max} = \frac{1}{4}\pi, \frac{5}{4}\pi$, respectively. If $\cos \delta < 0$ the positions of the minima and maxima simply exchange. Assuming $\rho \ll B_I/G$ the radial position of these extrema evaluates to

$$\rho_0 = \frac{1}{2G} \sqrt{B_{\text{RF}}^2 (1 - \cos \delta \sin(2\phi) + \sin \delta) - 2B_C^2} \quad (32)$$

with the critical field strength $B_C = 2\sqrt{B_I \frac{\hbar \Delta}{g_F \mu_B}}$ and the detuning $\hbar \Delta = |g_F \mu_B| B_I - \hbar \omega$. Hence for $\cos \delta > 0$ and $B_{\text{RF}} < \sqrt{\frac{2}{1 + \cos \delta + \sin \delta}} B_C$ or $\cos \delta < 0$ and $B_{\text{RF}} < \sqrt{\frac{2}{1 - \cos \delta + \sin \delta}} B_C$ solely a single minimum with respect to the radial coordinate can be achieved. For $\delta = \frac{3}{2}\pi$ in any case only a single minimum is found.

We now inspect the condition (14). For the current setup we find

$$\gamma_1 = \frac{g_F \mu_B B_{\text{RF}} G \rho}{\sqrt{2} \hbar \omega |\mathbf{B}_S(\mathbf{r})|} \cos \phi \quad \text{and} \quad \gamma_2 = \frac{g_F \mu_B B_{\text{RF}} G \rho}{\sqrt{2} \hbar \omega |\mathbf{B}_S(\mathbf{r})|} \sin \phi \quad (33)$$

which can in case of a resonant rf field ($g_F \mu_B B_{\text{RF}} \approx \hbar \omega$) be approximated by

$$\gamma_{1,2} \approx \frac{G \rho}{2 |\mathbf{B}_S(\mathbf{r})|} \approx \frac{1}{2} \frac{G \rho}{B_I} - \frac{1}{4} \left[\frac{G \rho}{B_I} \right]^3. \quad (34)$$

Thus if the splitting distance ρ_0 is kept small and at the same time the Ioffe field strength high the validity of the condition $\gamma_{1,2} \ll 1$ can be ensured.

B. Numerical wave packet propagation

To obtain exact results and in particular to estimate the quality of the adiabatic approach we will now perform a numerically exact wave packet propagation. Consider the wave packet $|\Psi(t)\rangle$ which we decompose according to

$$|\Psi(t)\rangle = \sum_{nmm_F} c_{nmm_F}(t) |m, n\rangle |m_F\rangle \quad (35)$$

where the functions $|m, n\rangle$ are the orthonormal eigenfunctions of a two-dimensional harmonic oscillator in Cartesian coordinates

$$|m, n\rangle = \frac{\sqrt[4]{M^2 \omega_x \omega_y}}{\sqrt{2^{m+n} \pi \hbar m! n!}} e^{-\frac{M}{2\hbar}(\omega_x x^2 + \omega_y y^2)} H_m \left(\sqrt{\frac{M \omega_x}{\hbar}} x \right) H_n \left(\sqrt{\frac{M \omega_y}{\hbar}} y \right). \quad (36)$$

The frequencies ω_x and ω_y can be regarded as parameters which can be adapted in order to improve the convergence of the numerical propagation [24]. To cover the spin space dynamics we utilize the spinor-orbitals $|m_F\rangle$, respectively. Inserting the state (35) into the Schrödinger equation (28) and multiplying by $\langle m'_F| \langle m', n'|$ from the left yields the set of ordinary differential equations

$$i \hbar \partial_t c_{nmm_F}(t) = \sum_{n'm'm'_F} \langle m'_F| \langle m', n'| H_{2\text{RF}}(t) |n, m\rangle |m_F\rangle c_{n'm'm'_F}(t) \quad (37)$$

which can now be used to propagate the coefficients $c_{nmm_F}(t)$ in time. For all practical purposes this system of first order differential equations has to be truncated yielding a set of equations of finite dimension. Then it can be solved by using standard numerical integration methods. In particular we have used a Runge-Kutta integrator with adaptive stepsize provided by the NAG library. This method is not norm-conserving. Thus we have to ensure the conservation of the norm at any time step which at the same time serves as a measure of the quality of the propagation. During the propagation we solely ramp up the rf field strength B_{RF} from zero to its final value. All other parameters remain unchanged. At $t = 0$ and consequently $B_{\text{RF}} = 0$ the Hamiltonian (27) resembles that of a stationary Ioffe-Pritchard trap. For a sufficiently large Ioffe field strength, i.e. $G \rho \ll B_I$, the ground state of an atom of mass M in this trap can be approximated by [24]

$$\Psi_0(x, y) = \langle \mathbf{r} | \Psi_0 \rangle = \sqrt{\frac{M \omega}{\pi \hbar}} \exp \left[-\frac{M \omega}{2 \hbar} (x^2 + y^2) \right] |m_F\rangle \quad (38)$$

with the trap frequency

$$\omega = G \sqrt{\frac{g_F \mu_B m_F}{M B_I}}. \quad (39)$$

Thereby we assume the atom to be in a hyperfine sub-state with $m_F g_F > 0$. For all numerical calculations presented in this work we use the wave function (38) as initial state, i.e. $|\Psi(x, y, t = 0)\rangle = |\Psi_0(x, y)\rangle$. In figure 1 we present

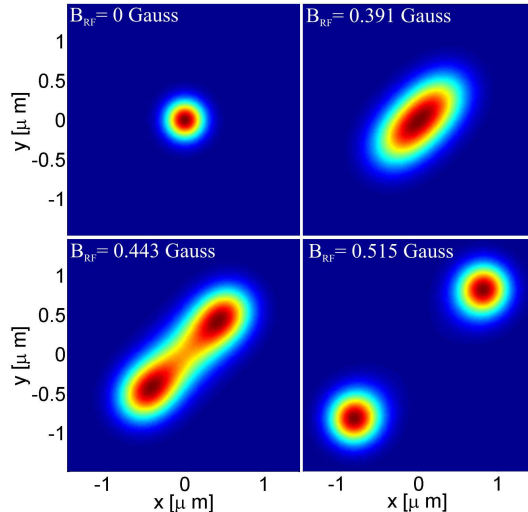


FIG. 1: Propagation of a wave packet from a single well into a double well for $G = 20$ T/m, $B_I = 0.75$ Gauss, $g_F = -\frac{1}{2}$, $m_F = -1$ and $\delta = \pi$. B_{RF} is linearly ramped from zero to 0.515 Gauss within 7.6 ms. The radio frequency is $\omega = 2\pi \times 500$ kHz. Shown is the probability density $|\Psi(x, y)|^2$.

the propagation of an atomic ^{87}Rb wave packet from the ground state in a Ioffe-Pritchard trap into a double well. The relative phase shift between the two rf fields is π . The atom is supposed to be in the upper branch of the $F = 1$ -manifold of the ground state, i.e. $g_F = -\frac{1}{2}$ and $m_F = -1$. We ramp the amplitude linearly from zero to 0.515 Gauss over a period of 7.6 ms. All other parameters remain at constant values $G = 20$ T/m, $B_I = 0.75$ Gauss. The wave packet propagation reproduces the results which one would expect from inspecting the adiabatic potentials. For $\delta = \pi$ the potential minima are located on the line defined by $x = y$. According to equation (32) the final splitting distance is $\rho_0 = 1.4 \mu\text{m}$ which is also quite well reproduced. For this value of ρ_0 the parameters $\gamma_{1,2}$ evaluate to approximately 0.25. Hence, although the condition $\gamma_{1,2} \ll 1$ is not strictly satisfied the adiabatic description appears to work quite well.

We now consider a relative phase shift of $\delta = \frac{\pi}{2}$ between the two rf fields. In this case the potential (31) becomes independent of the polar angle ϕ and hence rotationally symmetric. For our numerical wave packet propagation we start again in the ground state (38) and at zero rf amplitude. Subsequently we ramp the rf amplitude to 0.446 Gauss within 7.6 ms. This is done linearly at a constant rf frequency of $\omega = 2\pi \times 500$ kHz. The resulting probability density is depicted in figure 2. The initially Gaussian distribution is isotropically deformed until a ring-shaped wave function emerges. For the parameters given the final ring radius evaluates according to equation (32) to $\rho_0 = 1.08 \mu\text{m}$ which is in very good agreement with the numerical simulation (one finds $\gamma_{1,2} = 0.16$).

V. INTERFERENCE EXPERIMENTS IN AN RF INDUCED DOUBLE-WELL

The excellent performance of rf induced potentials for conducting interference experiments has been both demonstrated experimentally [16] and studied theoretically [17]. It was shown that by using the rf scheme splitting distances of only a few microns can be achieved. Such small splittings cannot be observed directly by means of absorption imaging. However, by switching off all magnetic fields (which is assumed to happen instantaneously) and after waiting a sufficiently long period of time the structure of the expanded cloud can be resolved. In case of an initially split cloud usually an interference pattern is observed [16].

We will now discuss how the nature of the rf potentials gives rise to a reduction of the interference contrast. Assuming a free propagation of the initial state being characterized by the wave function $\Psi(\mathbf{x}, t_0)$ we find the probability density

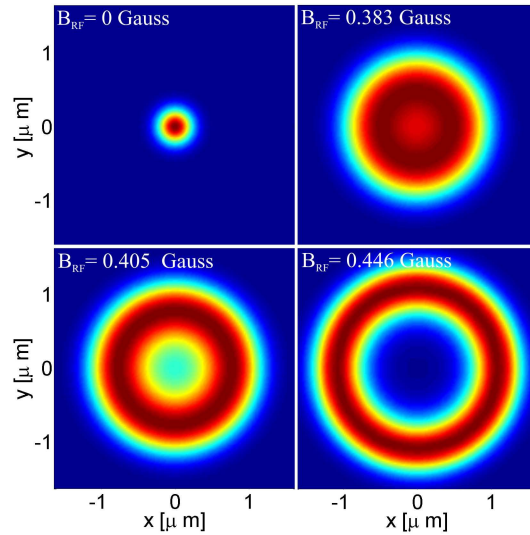


FIG. 2: Propagation of a wave packet from a single well into a ring potential for $G = 20$ T/m, $B_I = 0.75$ Gauss, $g_F = -\frac{1}{2}$ and $m_F = -1$. B_{RF} is linearly ramped from zero to 0.446 Gauss within 7.6 ms. The radio frequency is $\omega = 2\pi \times 500$ kHz. Shown is the probability density $|\Psi(x, y)|^2$.

after a time $t + t_0$

$$|\Psi(\mathbf{x}, t + t_0)|^2 = \frac{1}{(2\pi)^{2d}} \left[\frac{m\pi}{2\hbar|t - t_0|} \right]^d \left| \mathfrak{F} \left\{ \exp \left(\frac{im\mathbf{x}^2}{2\hbar|t - t_0|} \right) \times \Psi(\mathbf{x}, t_0) \right\} \left(\frac{m\mathbf{x}}{\hbar|t - t_0|} \right) \right|^2 \quad (40)$$

with d being the number of spatial dimensions considered and $\mathfrak{F}\{g(\mathbf{x}')\}(\mathbf{x})$ being the Fourier transform of the function $g(\mathbf{x}')$ evaluated at the position \mathbf{x} . If $|t - t_0|$ becomes large and the initial state is localized the position dependent phase factor $\exp\left(\frac{im\mathbf{x}^2}{2\hbar|t - t_0|}\right)$ becomes approximately uniform over the extension of $\Psi(\mathbf{x}, t_0)$ and can thus be taken out from the argument and put in front of the Fourier integral. In this case the the probability density after the time-of-flight period is simply the Fourier transform of $\Psi(\mathbf{x}, t_0)$. Since $\Psi(\mathbf{x}, t_0)$ is a spinor wave function the Fourier transform is to be taken of each spinor component separately. Hence one would expect the occupation of the individual spinor orbitals to have an effect on the interference pattern. For the purpose of demonstration we now consider the final state of the wave packet propagation which is shown in figure 1. In figure 3a we present the spin decomposition of this particular state. The probability amplitude seems to be randomly distributed over the three spinor orbitals.

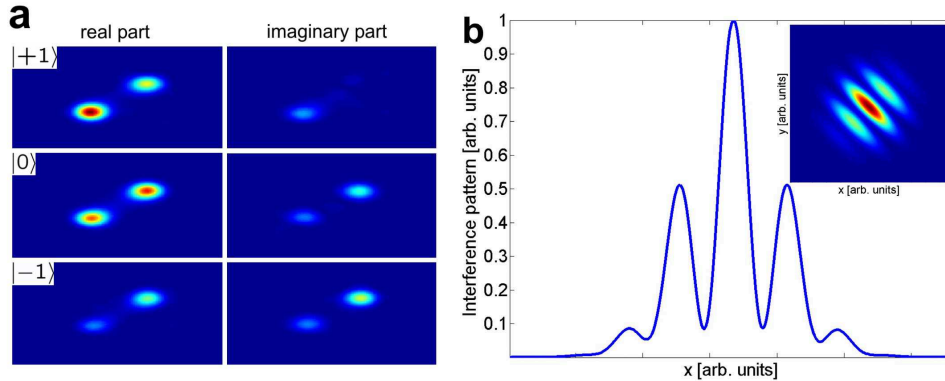


FIG. 3: **a**: Real and imaginary parts of the wave function components which occupy the spinor orbitals $|m_s\rangle$. The state shown is the final state of the propagation presented in figure 1. For each plot the same colormap was used. **b**: Cut along $x = y$ through the interference pattern after a time-of-flight experiment. The interference contrast is significantly smaller than 100%. This is essentially a consequence of the different spin states of the two interfering clouds.

None of the orbitals shows a spatially symmetric occupation like the squared modulus of the wave function which has

interesting consequences for the interference contrast. From the squared modulus of the final state's wave function (see figure 1) one would expect to achieve 100 % of contrast in the interference pattern, i.e. $\min |\Psi(\mathbf{x}, t + t_0)|^2 = 0$. The actual calculation of the interference pattern (3)b, however, yields a contrast of about 90 %. This modification of the interference pattern by the spatially asymmetric occupation of the spinor orbitals will be subject of the following discussion.

We focus on the rf double-well which is described by equation (31) if $\delta = 0$ or π . We consider the interference pattern that emerges if two completely separated clouds which are located in the two wells interfere. For the purpose of illustration we consider the one-dimensional dynamics along the axis which is defined through the position of the double-well minima $\pm x_0$ (see figure 4a). We further model our initial state according to

$$\Psi(\mathbf{x}, t = 0) = \frac{1}{\sqrt{2}} [\delta(x - x_0) |x_0\rangle_S + \delta(x + x_0) |-x_0\rangle_S]. \quad (41)$$

The spatial part of the two separated wave functions is described by delta functions. The spin is accounted for by

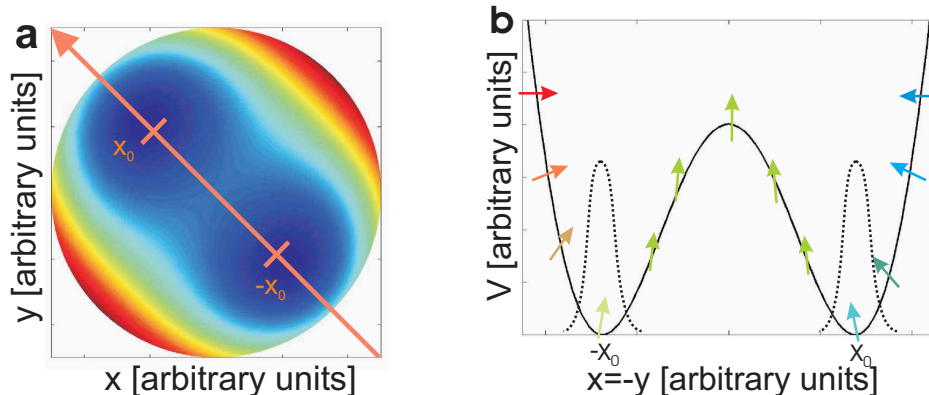


FIG. 4: **a**: Two-dimensional plot of the double well potential (31) for $\delta = 0$. In order to study the dependence of the interference contrast on the splitting distance $2x_0$ we consider only the 1-dimensional motion along the indicated axis. **b**: Sketch of the spin orientation in an rf double-well potential along the axis being shown in **a**. The spin orientation is assumed to follow adiabatically the local direction of the effective magnetic field. Hence the interference contrast of two interfering clouds depends in general on the relative orientation of the two spin vectors.

the spinor orbitals $|x\rangle_S$. For the Fourier transform of the state (41) one obtains

$$\Psi(k) = \frac{1}{\sqrt{2}} [\exp(ikx_0) |x_0\rangle_S + \exp(-ikx_0) |-x_0\rangle_S]. \quad (42)$$

Hence, according to equation (40) the probability density after a sufficiently long waiting period evaluates to

$$\begin{aligned} |\Psi(\mathbf{x}, t)|^2 &\approx \text{const} \times \left[2 + \exp\left(-2i\frac{mx}{\hbar t}x_0\right) \langle x_0 | -x_0\rangle_S + \exp\left(2i\frac{mx}{\hbar t}x_0\right) \langle -x_0 | x_0\rangle_S \right] \\ &\propto 1 + \text{Re} \{ \exp(i k_0 x) \langle -x_0 | x_0\rangle_S \} \end{aligned} \quad (43)$$

with $k_0 = 2\frac{mx_0}{\hbar t}$. If the shape of the spinor wave function was independent of the spatial position x_0 one would observe an interference pattern with 100 % contrast and a period of $\frac{2\pi}{k_0}$. In general, however, we find $|\langle -x_0 | x_0\rangle_S| \leq 1$ which is simply the result of the adiabatic alignment of the spin along the effective magnetic field vector which is illustrated in figure 4b. This means that the spin states of the two initial, now interfering, fragments were not identical. It is easily seen this effect to lead to a reduction of the interference contrast and to a variation of the global phase of the interference pattern.

To calculate the quantity $\langle -x_0 | x_0\rangle_S$ we use the unitary transformations which we have employed to achieve the adiabatic rf potentials. In the dressed frame the spinor wave function is independent of the spatial coordinate and will be characterized by $|\text{ad}\rangle$. To obtain the spin wave function in the lab frame $|x\rangle_S$ we have to apply the unitary transformations (3), (7), (10) and (20). After that we receive

$$|x\rangle_S = U_F(x)U_TU_RU_S(x)|\text{ad}\rangle. \quad (44)$$

Hence we find

$$\langle -x_0 | x_0\rangle_S = \langle \text{ad} | U_S^\dagger(-x_0)U_R^\dagger U_T^\dagger U_F^\dagger(-x_0)U_F(x_0)U_TU_RU_S(x_0) | \text{ad} \rangle \quad (45)$$

This expression simplifies considerably if we employ cylindrical coordinates. With $x_0 = (\rho_0, \phi = \frac{3\pi}{4})$ and $-x_0 = (\rho_0, \phi = \frac{7\pi}{4})$ we end up with

$$U_F^\dagger(-x_0)U_F(x_0) = \exp\left[i \arctan\left(\frac{G\rho_0}{B_I}\right) F_y\right] \exp[iF_z\pi] \exp\left[-i \arctan\left(\frac{G\rho_0}{B_I}\right) F_y\right]. \quad (46)$$

We now neglect the transformation U_T . Its effect is expected to be small since we consider the case $\gamma_n \ll 1$. Furthermore we note that

$$U_S(x_0) = U_S^\dagger(-x_0) = \exp[-i \arctan(\zeta(\rho_0)) F_y] \quad (47)$$

with

$$\zeta(\rho_0) = \frac{B_{RF}B_I}{2|\mathbf{B}_S(\rho_0)| \left[|\mathbf{B}_S(\rho_0)| - \frac{\hbar\omega}{|g_F\mu_B|}\right]} \approx |g_F\mu_B|B_{RF} \left[\frac{1}{2\hbar\Delta} - \frac{\hbar\Delta + |g_F\mu_B|B_I}{4} \left[\frac{G\rho_0}{\hbar\Delta B_I} \right]^2 \right]. \quad (48)$$

In case of a resonant rf one hence finds as a zeroth order approximation $\zeta(\rho_0) \approx \frac{B_{RF}}{2B_I}$. Putting everything together we finally arrive at

$$\langle -x_0 | x_0 \rangle_S = \langle \text{ad} | U_S^\dagger(x_0) \exp\left[i\pi \frac{B_I F_z - G\rho_0 \cos(\omega t) F_x + G\rho_0 \sin(\omega t) F_y}{|\mathbf{B}_S(\rho_0)|} \right] U_S^\dagger(x_0) | \text{ad} \rangle. \quad (49)$$

For a $F = 1/2$ particle in its trapped adiabatic state $|\text{ad}\rangle = |m_F = \frac{1}{2}\rangle$ one finds

$$\langle -x_0 | x_0 \rangle_S = \frac{1}{|\mathbf{B}_S(\rho_0)|} \left[iB_I - \frac{\zeta(\rho_0)}{\sqrt{1 + \zeta^2(\rho_0)}} G\rho_0 \sin(\omega t) \right]. \quad (50)$$

Apparently the overlap $\langle -x_0 | x_0 \rangle_S$ is not only a function of the relative displacement of the two atom clouds but also a function of the time t . This, however, implies the interference contrast to depend on the actual phase of the rf field.

Evaluating the interference term in equation (43) we finally obtain

$$\text{Re}\{\exp(i k_0 x) \langle -x_0 | x_0 \rangle_S\} = -\frac{B_I}{|\mathbf{B}_S(\rho_0)|} \sin(k_0 x) - \frac{\zeta(\rho_0)}{\sqrt{1 + \zeta^2(\rho_0)}} \frac{G\rho_0}{|\mathbf{B}_S(\rho_0)|} \sin(\omega t) \cos(k_0 x). \quad (51)$$

For the calculation in case of $F > 1/2$ the results given in appendix A can be used. The general structure of

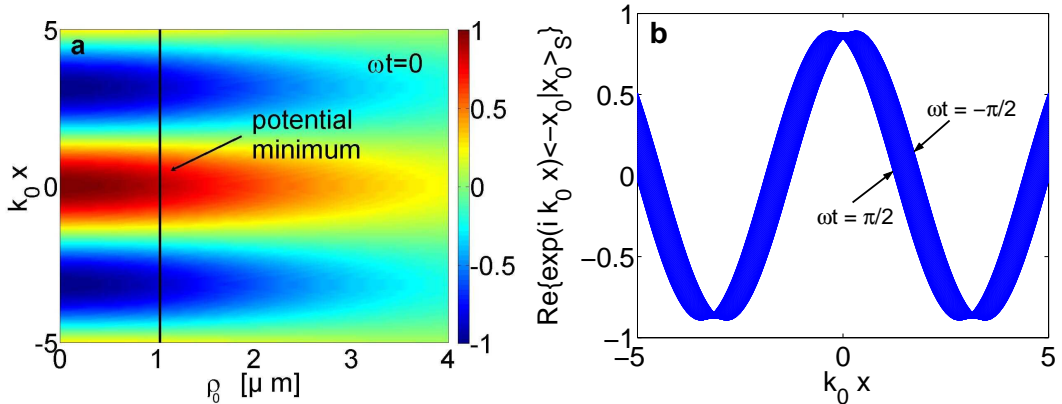


FIG. 5: **a**: Contrast pattern along the axis connecting the two potential minima of the double-well (see figure 4). The same parameters as in figure 1 have been used. The snapshot is taken at $\omega t = 0$. The position of the potential minimum is indicated by the vertical line. The interference contrast decreases as ρ_0 increases. For $\rho \rightarrow \infty$ the contrast goes to zero as both wave packets occupy orthogonal spin states. **b**: Time dependence of the interference if both wave packets are released from the double-well minima. One can clearly recognize the dependence of the interference pattern on the rf phase.

the interference term is similar for all cases. One encounters a time-independent term which accounts for the static components of the magnetic field and an oscillating one which gives rise to a temporal modulation of the interference

pattern. This can be interpreted as the effect of the micro-motion of the atoms within the adiabatic potentials similar to trapped ions in a Paul-trap. Using equation (51) one finds a phase variation of

$$\Delta\phi = 2 \arctan \left[\frac{\zeta(\rho_0)}{\sqrt{1 + \zeta^2(\rho_0)}} \frac{G\rho_0}{|\mathbf{B}_S(\rho_0)|} \right] \approx 2 \left[\frac{G\rho_0}{B_I} \right] \left[1 + \left[\frac{2\hbar\Delta}{g_F\mu_B B_{RF}} \right]^2 \right]^{-\frac{1}{2}} \quad (52)$$

over one rf oscillation period. For a spin 1 particle this rf phase dependence of the interference pattern is shown in figure 5b. The right-hand side of equation (52) is the leading order term in $\frac{G\rho_0}{B_I}$. Hence the phase oscillations can be suppressed by keeping the ratio $\frac{G\rho_0}{B_I}$ small which is in agreement with the previous assumption $G\rho \ll B_I$.

The above consideration assumes an immediate switch-off of all external magnetic fields before the expansion of the matter wave. However, for all practical purposes there is always a finite switch off time. One might think of switching off the fields such that finally all atoms are rotated into the same spin state but the spatial shape of the matter wave remains unchanged. To succeed in establishing such a sophisticated switching-off procedure seems to be unlikely since at each spatial and temporal position the atomic spin state had to be rotated differently.

VI. SUMMARY AND CONCLUSION

We have presented the theoretical foundations for the description of rf induced adiabatic potentials. Starting from a Hamiltonian that takes into account the coupling of a single hyperfine manifold to an external field we have carried out a number of unitary transformations. After performing the rotating wave approximation and neglecting the non-adiabatic couplings which emerge from the transformed kinetic energy we have received the corresponding adiabatic potential surfaces.

To demonstrate the power of this rf induced dressed adiabatic potentials we have discussed a simple field configuration consisting of a static Ioffe-Pritchard trap and two orthogonal homogeneous rf fields. Our analytical calculations have shown that by tuning the strength of the rf fields a smooth transition from a single well into a double well is achievable. This transition can be easily exploited to split a cloud of ultracold atoms. By introducing a relative phase shift between the two rf fields furthermore a transition from a double well to a ring potential can be performed. For our considerations we have mainly focussed on ^{87}Rb in the $F = 1$ hyperfine ground state. For this species the analytical results have been verified by a numerical wave packet propagation which was conducted using a linear single particle Schrödinger equation and the original Hamiltonian. For typical experimental parameters these numerical results have been shown to be in very good agreement with the ones obtained from the analytic adiabatic approach.

Finally we have discussed interference experiments carried out in a rf double-well potential. Since the trapping potential is a consequence of a spin-field coupling the spin state of a trapped atom cloud depend on its actual spatial position. This essentially leads to a spatially asymmetric distribution of the atomic wave function within the individual spinor orbitals and an inevitable reduction of the interference contrast. Moreover, the rf field imposes a high-frequency oscillation on the interference fringes which is reminiscent of a micromotion. The magnitude of these effects can be well controlled by appropriately tuning the experimental parameters such as the Ioffe field strength and the detuning.

APPENDIX A: $\langle -x_0 | x_0 \rangle_S$ IN CASE OF $F \geq \frac{1}{2}$

Overlap of the spin wave functions for atoms in the $F = \frac{1}{2}, 1, \frac{3}{2}, 2$ -state calculated according to equation (49):

$$\langle -x_0 | x_0 \rangle_S = \left[\frac{1}{|\mathbf{B}_S(\rho_0)|} \left(iB_I - \frac{\zeta(\rho_0)}{\sqrt{1 + \zeta^2(\rho_0)}} G\rho_0 \sin(\omega t) \right) \right]^{2F}. \quad (A1)$$

The atom is assumed to occupy the maximal stretched stated, i.e. $m_F = F$. Like in the $F = \frac{1}{2}$ -case (equation (50)) we find a static and a time-dependent part. Here, the latter has contribution of terms that oscillate at the frequencies $\omega, \dots, 2F \times \omega$.

[1] A.L. Migdall *et al.*, Phys. Rev. Lett. **54**, 2596 (1985)

[2] T. Bergeman, G. Erez, and H.J. Metcalf, Phys. Rev. A **35**, 1535 (1987)

[3] J. Schmiedmayer, Phys. Rev. A **52**, R13 (1995)

- [4] R. Folman *et al.*, Adv. At. Mol. Opt. Phys. **48**, 263 (2002)
- [5] D. Cassettari *et al.*, Phys. Rev. Lett. **85**, 5483 (2000)
- [6] F. Schreck *et al.*, Phys. Rev. Lett. **87**, 080403 (2001)
- [7] I. Lesanovsky and P. Schmelcher, Phys. Rev. A **71**, 032510 (2005)
- [8] J. Fortagh *et al.*, Phys. Rev. Lett. **81**, 5310 (1998)
- [9] W. Hänsel, J. Reichel, P. Hommelhoff, and T. W. Hänsch, Phys. Rev. A **64**, 063607 (2001)
- [10] E.A. Hinds, C.J. Vale, and M.G. Boshier, Phys. Rev. Lett. **86**, 1462 (2001)
- [11] E. Andersson *et al.*, Phys. Rev. Lett. **88**, 100401 (2002)
- [12] P. Hommelhoff *et al.*, New J. Phys. **7**, 3 (2005)
- [13] J. Estève *et al.*, Eur. Phys. J. D **35**, 141 (2005)
- [14] Zobay, O. and Garraway, B. M., Phys. Rev. Lett. **86**, 1195-1198 (2001)
- [15] Zobay, O. and Garraway, B. M., Phys. Rev. A **69**, 023605 (2004)
- [16] T. Schumm *et al.*, Nat. Phys. **1**, 57 (2005).
- [17] I. Lesanovsky *et al.* Phys. Rev. A **73**, 033619 (2006)
- [18] T. Fernholz *et al.*, physics/0512017 (2005)
- [19] Ph. W. Courteille *et al.*, J. Phys. B **39** 1055 (2006)
- [20] O. Morizot *et al.*, physics/0512015 (2005)
- [21] M. R. Andrews *et al.*, Science **31**, 637 (1997)
- [22] M. Albiez *et al.*, Phys. Rev. Lett. **95**, 010402 (2005)
- [23] D.E. Pritchard *et al.*, Phys. Rev. Lett. **51**, 1336 (1983)
- [24] J. Bill, M.-I. Trappe, I. Lesanovsky and P. Schmelcher, Phys. Rev. A (2006)